

RSC Advances



This is an *Accepted Manuscript*, which has been through the Royal Society of Chemistry peer review process and has been accepted for publication.

Accepted Manuscripts are published online shortly after acceptance, before technical editing, formatting and proof reading. Using this free service, authors can make their results available to the community, in citable form, before we publish the edited article. This *Accepted Manuscript* will be replaced by the edited, formatted and paginated article as soon as this is available.

You can find more information about *Accepted Manuscripts* in the [Information for Authors](#).

Please note that technical editing may introduce minor changes to the text and/or graphics, which may alter content. The journal's standard [Terms & Conditions](#) and the [Ethical guidelines](#) still apply. In no event shall the Royal Society of Chemistry be held responsible for any errors or omissions in this *Accepted Manuscript* or any consequences arising from the use of any information it contains.

Recycling of waste printed circuit boards into ion exchange resin

Jianqiu Zhang^{a*}, Tao Tian^a, Jinyang Chen^{a*}, Jianhua Zu^b, Yangjun Wang^a

Abstract

Recycling the nonmetal components of waste printed circuit boards (WPCBs), mainly thermosetting epoxy resins (TEPRs), is quite difficult because they are insoluble and inflexible. We report a new method to convert TEPRs into ion exchange resin by treatment with sulphuric acid and the equilibrium ion exchange capacity (IEC) of the produced sample is $1.63 \text{ meq}\cdot\text{g}^{-1}$. FTIR indicated that TEPRs were modified by sulphuric acid and X-ray photoelectron spectroscopy (XPS) verified that sulfonic acid group ($-\text{SO}_3^-$) was introduced. The produced ion exchange resin was stable up to $200 \text{ }^\circ\text{C}$ by TG-DTG analysis. The maximum adsorption capacities for Cu(II) and Ca(II) were 23.30 and $56.27 \text{ mg}\cdot\text{g}^{-1}$, respectively. The Langmuir model gave a better fit for adsorption than the Freundlich model. The activation energies (E_a) were 21.18 and $48.53 \text{ kJ}\cdot\text{mol}^{-1}$ for Cu(II) and Ca(II), respectively, with pseudo-second-order kinetics.

Keywords: WPCBs, Recycling, Sulfonation, Ion exchange resin, Isotherms, Kinetics

1. Introduction

The printed circuit board (PCB) is the foundation of the electronic industry: an essential component of every electrical and electronic device. The rapid development of the electronic industry has resulted in a significant increase in the production of waste printed circuit boards (WPCBs)^{1,2}. In recent years, the recovery of metals from WPCBs has received more and more attention because of their high metal content, which may exceed that of some mineral deposits. This makes WPCBs an attractive secondary source of metals³⁻⁸. Other than metals, WPCBs are mainly mixtures of polymers and glass fibres⁹. The most common polymers in WPCBs are thermosetting epoxy resins (TEPRs), such as bromine epoxy resin, which is used as a fire retardant^{10,11}. However, because TEPRs are insoluble and infusible, it is difficult to treat and recycle. The increase in TEPR wastes has resulted in health problems and

environmental pollution. There is thus an urgent need to recycle or reuse TEPRs.

Ion exchange resins based on polystyrene are capable of ion exchange mainly because of sulfonic acid groups ($R-SO_3H$), R is the network structure from of the resin frame part. The chemical structure of TEPRs, including the main aromatic ring, is shown in Fig. 1. It is possible to introduce functionalities, such as sulfonic acid groups, by sulfonation¹². In the sulfonation of TEPRs, an $-SO_3H$ group is attached to the aromatic ring. Ion exchange resins consisting of sulfonated TEPRs (S-TEPRs) have a fixed negative charge ($-SO_3^-$) that allows mobile cations (H^+) to migrate while excluding co-ions and the sulfonated thermosetting epoxy resins (S-TEPRs) can be cation exchange resins.

Here we present the new process using sulfonation to recycle TEPRs into ion exchange resins (S-TEPRs). We measured several properties of the products: ion exchange capacity (IEC), swelling degree (SD) or water uptake (WU). Resins were characterized by Fourier transform infrared spectroscopy (FTIR), elemental analysis, thermal analysis (TG-DTG) and X-ray photoelectron spectroscopy (XPS). To investigate the ion exchange process, the product was used to remove Cu(II) and Ca(II) and ion exchange isotherms and kinetics were determined.

2. Experimental

2.1 Materials

The aTEPRs powder was obtained from the Shanghai Solid Waste Manage Center. The bTEPRs powder was manufactured in the lab from a 50 wt% E51/Polyamide Resin, cured at 60 °C and 12 h, grinded into powder of approximately 1 mm in diameter. The 732 phenylethylene ion exchange resin (732 IER), $CuSO_4$, $CaCl_2$ and 98% (wt.%) sulphuric acid were provided by Sinopharm Chemical Reagent Co., Ltd. (China). E51 and polyamide resin were provided by Hong Kong Honour Rich Decoration Material International Group Limited.

2.2 Sulfonation

The aTEPR and bTEPR powders were dried in a vacuum oven at 100 °C for 48 h. Sulfonation of the aTEPRs and bTEPRs were carried out with the following steps: (1) 10 g TEPRs powder was added to 100 mL 98 % sulfuric acid and the mixture was

stirred vigorously at 85 °C for 360 min; (2) A large excess of ice water was added to stop the sulfonation and cause the precipitation of sulfonated TEPRs under continuous mechanical stirring; (3) The sulfonated TEPR precipitation was then filtered and washed with deionized water until the pH 7. The obtained sulfonated TEPRs powder was dried in an oven at 60 °C for 24 h.

2.3 Ion exchange capacity (IEC)

IEC ($\text{meq}\cdot\text{g}^{-1}$) was determined by acid–base titration. First H^+ type resin was neutralized with excess aqueous NaOH, converting the resin into Na^+ type. Then the excess NaOH was determined by neutralization to pH 7 with dilute HCl solution. Thus IEC was calculated by Eq. (1)¹³:

$$IEC = \left(\frac{(MV)_{\text{NaOH}} - (MV)_{\text{HCl}}}{m_{\text{resin}}} \right) \times 1000 \quad (\text{meq} / \text{g}) \quad (1)$$

M and V are the molar concentration and volume of the solutions, respectively, while m_{resin} is the weight of the products (H^+ type).

2.4 Characterization

FTIR spectra were obtained on an Avatar 370 FTIR spectrometer with KBr powder. TG–DTG was obtained on a Netzsch STA 409 PC instrument at a rate of 10 °C/min under nitrogen atmosphere up to 900 °C.

WU and SD were calculated from Eq. (2)¹⁴.

$$\text{WU or SD} = \frac{G_s - G_d}{G_d} \times 100\% \quad (2)$$

Where G_s is the weight of swollen powder and G_d is the weight of dry powder.

X-ray photoelectron spectroscopy (XPS) was performed on an ESCALAB 250Xi (Thermo Fisher Scientific China Ltd) and the data were analysed using Avantage software.

2.5 Ion exchange isotherms and kinetics

To obtain the ion exchange isotherms and kinetics of S-bTEPRs, the resins were washed with HCl and NaOH, converted to the Na^+ type and dried in an oven at 60 °C to a constant weight. Cu(II) and Ca(II) solutions ($600 \text{ mg}\cdot\text{L}^{-1}$) were prepared by

dissolving CuSO_4 or CaCl_2 in deionised water. The 0.5 g resin and 50 ml Cu(II) or Ca(II) solution ($600 \text{ mg}\cdot\text{L}^{-1}$) were put into 2Hz vibration frequency vessel and adjusted to pH 9 with NaOH to conduct adsorption process at ambient temperature. The metal concentration in the solution was then analysed by ICP. The adsorption capacity (q_t) of the resin was obtained as follows¹⁵:

$$q_t = \frac{(C_o - C_t) \times v}{m} \quad (3)$$

Where v is the volume of solution (L); m is the mass of resin (g); C_o and C_t are ion concentrations ($\text{mg}\cdot\text{L}^{-1}$) at initial condition and adsorption time t ; and q_t is the adsorption capacity ($\text{mg}\cdot\text{g}^{-1}$).

3 Results and discussion

3.1 Photographs and ion exchange capacity of prepared S-TEPRs

Two typical TEPRs and their sulfonated products with 98 % sulphuric acid at 85 °C for 360 min are shown in Fig. 2. It shows that aTEPRs turns the color of yellow to dark brown after sulfonation and the main reason is that the aTEPRs was obtained from the Shanghai Solid Waste Manage Center, which has some impurity, with 98 % sulfuric acid the impurity may be oxidized to become brown. The bTERPs is pure E51/polyamide resin and its color becomes dark from transparent light yellow to reddish brown should be the conjugation of S=O in $-\text{SO}_3^-$ with benzene ring with the addition of $-\text{SO}_3^-$ groups to the benzene ring of product, indicating the sulfonation indeed took place.

The most important parameter of ion exchange resins is IEC. Fig. 3 shows the IEC of 732 IER, S-aTEPRs and S-bTEPRs at ambient temperature. It shows that IEC increases rapidly in a relatively short time. However, the increase in IEC become slowly when exchange time is prolonged. The IEC reaches a maximum at 120 min and as for 732 IER, S-bTEPRs and S-aTEPRs the values are 2.21, 1.98, and 1.63 $\text{meq}\cdot\text{g}^{-1}$, respectively. The IEC maintained a relatively stable value after 120 min, indicating that it reaches equilibrium.

Table 1 shows the adsorption properties of the samples. The equilibrium IEC of S-aTEPRs and S-bTEPRs are 73.76 and 89.29% for a value of 732 IER, respectively.

The WU (SD) of S-aTEPRs is lower than that of S-bTEPRs and 732 IER, which may be due to glass fibres. It is obvious that S-aTEPRs has excellent ion exchange capacity and has a greatly potential application.

3.2 Characteristics of the products

The FTIR spectra of bTEPRs and S-bTEPRs are shown in Fig. 4. The peaks at 2925 cm^{-1} and 2856 cm^{-1} represent the saturated C–H stretching vibrations of epoxy resin, which may be associated with methyl and methylene groups. Absorbance peaks of aromatic C=C stretching appears at 1509 cm^{-1} and 1459 cm^{-1} . The peak at 1550 cm^{-1} represents the amide curing agent. The peak at approximately 1240 cm^{-1} confirms the presence of C–O–C structure. In many case, strong acid caused broken of C–O–C bond, however, the results show that there are still a lot of these bonds after the sulfonation process, which because the structure is 3D net-like structure and only a part of this structure on the surface is broken during sulfonation. This little surface breakdown of C-O-C has little effect on ion exchange capacity of the recycling IER from waste WPCBs.

Comparing the FTIR spectra of bTERPs and S-bTEPRs, there are noticeable differences in the spectra. The presence of a new peak at approximately 1037 cm^{-1} is assigned to the symmetric and asymmetric stretching vibrations of $-\text{SO}_3\text{H}$ groups in S-bTEPRs. That the absorbance at approximately 3500 cm^{-1} representing the stretching vibration of O–H groups in S-bTEPRs is wider and stronger than in bTERPs should be due to the addition of $-\text{SO}_3\text{H}$ in S-bTEPRs, which cause the formation of intermolecular hydrogen bonding between SO_3H groups and absorbed water molecules¹⁶. The result shows that the bTEPRs has been added $-\text{SO}_3\text{H}$ group after sulfonation.

The thermal analysis of ion exchange resins has two main objects. One is to study the thermal properties of the resin to determine the thermal stability and degradation temperature^{17, 18}. The other important object is to characterize the resin¹⁹. Fig. 5 shows the TG of 732 IER and S-aTEPRs and it is clear that there are three steps in the decomposition curves of both samples. The first step is almost a level line up to the temperatures of 185 for 732 IER and 192 °C for S-aTEPRs, indicating that they

are stable less than 200 °C. The second step shows obvious weight loss starting at approximately 280 up to 487 for 732 IER and 465 °C for S-aTEPRs owing to the decomposing of the molecular structure. Then the third step starts continuous weight loss up to 800 °C till totally carbonization. Comparing with 732 IER, The more residual of S-aTEPRs (approximately 20%) may be due to glass fibres.

Figs. 6 and 7 show the TG-DTG of bTEPRs and S-bTEPRs, respectively. From room temperature to 250 °C, comparing the weight loss in Fig. 7 with Fig. 6, an obvious weight loss step can be observed from 25 to 200 °C in Fig. 7 which should be the loss of water combining with -SO₃H group in S-bTERPs. Fig. 6 shows significant weight loss at 435 °C; however, significant weight loss from S-bTEPRs presents at 310, 346 and 428 °C. It indicates that the two processes of decomposition are completely different and the reason should be due to the decomposition of the addition of -SO₃H group of S-bTEPRs.

The products of different weight loss steps for S-bTEPRs were analysed by FTIR, as shown in Fig. 8. Comparing the first step of no weight loss with initial sample, there is no obvious change and the elemental composition indicates that the C and S is unchanged, while the O and H has some decrease, as shown in Table 2. This may be due to evaporation of bound moisture in -SO₃H group resulting in weight loss of 5.27%.

As for the second step with weight loss, the characteristic C–S absorption peak at approximately 609 cm⁻¹ decreases significantly, indicating the breakdown of partial C–S bonds between sulfonic acid groups and phenyl rings²⁰. Elemental analysis shows a significant weight loss of the S and O, indicating the decomposition of -SO₃H group. Furthermore, as for C, there is also some weight loss which indicates that the carbon linkage molecular structure also decomposes. In the third step, the peaks of characteristic –CH₂– and phenyl ring disappear, indicating that S-bTEPRs is decomposed completely. This is accorded with the corresponding significantly decrease of C, H, O and S.

To confirm that the sulfonated group is covalently bonded to the bTEPR after sulfonation, XPS measurement of bTEPRs and S-bTEPRs were carried out and the

XPS wide scan spectra are shown in Fig. 9. In the bTEPRs and S-bTEPRs samples, a strong peak at approximately 285 eV (corresponding to C, 1 s), a weak peak at approximately 400 eV (corresponding to N, 1 s), and a strong peak at 533 eV (corresponding to O, 1 s) are all observed. However, a new peak for sulphur (S, 2p, 168eV) is observed originated from -SO₃H groups in S-bTEPRs and it is shown obviously in Fig. 10, indicating successful sulfonation to produce S-bTEPRs. The binding energies and elemental compositions are summarized in Table 3 and it shows that the content of S in S-bTEPRs is 8.58%, indicating sulfonation of S-bTEPRs from bTEPRs.

The XPS narrow scan C 1s scan spectra and fit curves for bTEPRs, along with the XPS narrow scan C 1s and S 2p spectra and fit curves for S-bTEPRs, are shown in Fig. 11. Comparing the C 1s fit curves of a with b, there is one new peak at approximately 285.5 eV and it is attributed to the C-S bond of the sulfonated skeleton. The most important information comes from S 2p spectrum and fit curves for S-bTEPRs in Fig. 11(c). The spectrum is deconvoluted into two peaks at 168.1 and 169.2 eV which be assigned to the 2p_{3/2} and 2p_{1/2} of sulphur in a high oxidation state, i.e., sulfonic acid groups (-SO₃⁻)²¹.

3.3 Ion exchange isotherms and kinetics of S-bTEPRs

3.3.1 Ion-exchange isotherms

The most powerful tools for the analysis of adsorption processes are isotherms and the Langmuir and Freundlich isotherm models are widely used.

The Langmuir isotherm is expressed as^{22,23}:

$$\frac{C_e}{q_e} = \frac{C_e}{Q_0} + \frac{1}{Q_0 b} \quad (5)$$

Where C_e is the equilibrium concentration (mg·L⁻¹), q_e is the solid adsorbate concentration at equilibrium (mg·g⁻¹), Q_0 is theoretical monolayer adsorption capacity (mg·g⁻¹) and b is related to the energy of adsorption (L·mg⁻¹).

The Freundlich isotherm model is expressed as^{23,24}:

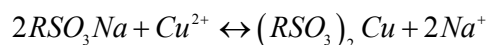
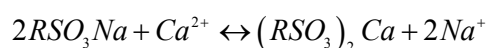
$$\log q_e = \log k_f + (1/n) \log C_e \quad (6)$$

Where k_f is adsorption capacity and n is related to the intensity of adsorption.

The Langmuir isotherm describes mono-layer adsorption on a homogenous surface and the Freundlich isotherm is a satisfactory empirical isotherm used for non-ideal adsorption on heterogeneous surface²⁴.

Figs. 12 and 13 show the Langmuir and Freundlich adsorption of Cu(II) and Ca(II) and their adsorption constants evaluated from isotherms are given in Table 4. The correlation coefficients of Cu(II) and Ca(II) of the Langmuir are 0.9981 and 0.9983 which are more perfect than corresponding 0.7855 and 0.8476 of Freundlich. The result indicates that the Langmuir isotherm model is a better fit to the equilibrium adsorption data.

As for the IER with the $-\text{SO}_3\text{Na}$ group which is the functional group grafted on the surface, the Cu(II) and Ca(II) will take place of Na^+ during the ion exchange process. The ion exchange reactions occurring in the Ca^{2+} and Cu^{2+} solution can be represented by the following reactions.



Obviously, the adsorption is chemical adsorption and thus the mono-layer Langmuir model is more suitable.

3.3.2 Ion-exchange kinetics

Experiments were carried out at 289-338 K to understand the ion-exchange kinetics. Based on the previous similar works²⁵⁻²⁸, it can assume that the ion-exchange kinetics is pseudo second-order reaction relative to the adsorbed amount.

The pseudo-second-order equation is expressed as:

$$\frac{t}{q_t} = \frac{t}{q_e} + \frac{1}{k_1 q_e^2} \quad (7)$$

Where k_1 (min^{-1}) is the rate constants of the second-order adsorption, q_e is the equilibrium adsorption capacity and q_t is the amount adsorbed at time “ t ”.

Plots of t/q_t against “ t ” at 298-338 K for the second-order adsorption are shown in

Fig. 14. The results provide the adsorption rate constants k_1 and q_e values from the slope and intercept in Table 5. The calculated q_e from the second-order kinetic model corresponded very well with experimental values, with $R^2 > 0.99$. It is obvious that the pseudo-second-order model provides a perfect fit of the experimental data and thus, the kinetics model is reliable and suitable.

The rate constant k can be expressed in Arrhenius form of $\ln k = -(E_a/RT) + \ln A$, where A is the pre-exponential factor, E_a is the activation energy ($\text{J}\cdot\text{mol}^{-1}$), R is the universal gas constant ($8.314 \text{ J}\cdot\text{mol}^{-1}\cdot\text{K}^{-1}$), and T is the temperature (K). Then according to Arrhenius equation, the line fitting relation of $\ln k$ and $1/T$ gives apparent adsorption activation energy E_a and Arrhenius pre-exponential factor A .

The relation of linearly fit of adsorption rate constant k_1 and temperature is shown in Fig. 15. According to Arrhenius equation, the linear fitting relation of $\ln k_1$ and $1000/T$ gives that the apparent adsorption activation energy (E_a) for the adsorption of Cu(II) and Ca(II) on S-bTEPRs are 21.18 and 48.53 $\text{kJ}\cdot\text{mol}^{-1}$, respectively. Thus, the adsorption kinetic equations are shown as Eqs. (8) and (9).

$$k_{1,Cu} = 0.2515 \times \exp\left(\frac{-21.18 \times 10^3}{8.314 \times T}\right) \quad \text{for Cu} \quad (8)$$

$$k_{1,Ca} = 0.6104 \times \exp\left(\frac{-48.53 \times 10^3}{8.314 \times T}\right) \quad \text{for Ca} \quad (9)$$

The positive values of E_a suggest that higher temperature favours adsorption and that the adsorption is endothermic.

4 Conclusions

Thermosetting epoxy resins, nonmetal materials from WPCBs, were transformed into ion exchange materials using sulphuric acid. The equilibrium IEC is 1.63 $\text{mmol}\cdot\text{g}^{-1}$ and it can be used safely below 200 °C. The process is a low cost method to produce high-value product for the recycling of waste WPCBs.

The produced IER is an effective adsorbent for the removal of Cu(II) and Ca(II) and the Langmuir isotherm model is suitable for the adsorption. The adsorption capacity for Cu(II) and Ca(II) calculated from the Langmuir model are 56.27 and 23.30 mg·g⁻¹, respectively. The adsorption kinetics of Cu(II) and Ca(II) are suitable for pseudo-second-order rate model and the apparent E_a for Cu(II) and Ca(II) are 21.18 and 48.53 kJ·mol⁻¹, respectively.

Acknowledgements

This research was supported by the National Natural Science Foundation of China (No. 20777048, 91226111) and the Program for Innovative Research Team in University (No. IRT13078).

Notes and References

^a School of Environmental and Chemical Engineering, Shanghai University, Shanghai 200444, China

^b School of Nuclear Science and Engineering, Shanghai Jiao Tong University, Shanghai, 200240 china

- 1 W.J. Hall, P.T. Williams, *Resour. Conserv. Recy.*, 2007, **51**, 691–709.
- 2 P. Zhu, G.B. Gu, *Chinese Journal of Rare Metals*. (in Chinese), 2002, **26**, 214–216.
- 3 Y. Zhou, K. Qiu, *J. Hazard. Mater.*, 2010, **175**, 823–828.
- 4 I.D. Marco, B.M. Caballero, M.J. Chomón, M.F. Laresgoiti, A. Torres, G. Fernández, S. Arnaiz, *J. Anal. Appl. Pyrol.*, 2008, **82**, 179–183.
- 5 C. Quan, A. Li, N. Gao, *Waste Manage.*, 2009, **29**, 2353–2360.
- 6 J.H. William, T.W. Paul, *Resour. Conserv. Recy.*, 2007, **51**, 691–709.
- 7 C. Hung-Lung, L. Kuo-Hsiung, L. Mei-Hsiu, C. Ting-Chien, M. Sen-Yi, *J. Hazard. Mater.*, 2007, **149**, 151–159.
- 8 F. Barontini, V. Cozzani, *J. Anal. Appl. Pyrol.*, 2006, **77**, 41–55.
- 9 J. Li, H.Z. Lu, J. Guo, Z.M. Xu, R.H. Zhou, *Environ. Sci. Technol.*, 2007, **41**, 1995–2000.
- 10 J. Guan, Y.S. Li, M.X. Lu, *J. Anal. Appl. Pyrol.*, 2008, **83**, 185–189.
- 11 A.C. Kasper, G.B.T. Berselli, B.D. Freitas, J.A.S. Tenório, A.M. Bernardes, H.M. Veit, *Waste Manage.*, 2011, **31**, 2536–2545.
- 12 H.C. Lee, H.S. Hong, Y.M. Kim, S.H. Choi, M.Z. Hong, H.S. Lee, K. Kim, *Electrochim. Acta*,

- 2004, **49**, 2315–2323.
- 13 R.Y.M. Huang, P. Shao, C.M. Burns, X. Feng, *J. Appl. Polym. Sci.*, 2001, **82**, 2651–2660.
- 14 F. Barroso-Bujans, R. Verdejo, A. Lozano, J.L.G. Fierro, M.A. Lopez-Manchado, *Acta Mater.*, 2008, **56**, 4780–4788.
- 15 F. Gode, E. Pehlivan, *J. Hazard. Mater.*, 2006, **136**, 330–337.
- 16 P. Xing, G.P. Robertson, M.D. Guiver, S.D. Mikhailenka, K. Wang, S. Kaliaguine, *J. Membr. Sci.*, 2004, **229**, 95–106.
- 17 S. M. Dakka, *J. Therm. Anal. Calorim.*, 2003, **74**, 729–734.
- 18 S.M. Dakka, *J. Therm. Anal. Calorim.*, 2003, **73**, 17–24.
- 19 D. Chambree, C. Iditoiu, E. Segal and A. Cesrao, *J. Therm. Anal. Calorim.*, 2005, **82**, 803–811.
- 20 H. Qian, Q.J. Peng, J.W. Zhang, *Ion Exchange and Adsorption* (in Chinese), 2012, **28**, 413–422.
- 21 M. M. Nasef, H. Saidi, *Appl. Surf. Sci.*, 2006, **252**, 3073–3084.
- 22 I. Langmuir, *J. Am. Chem. Soc.*, 1916, **38**, 2221–2295.
- 23 S. S. Gupta and K.G. Bhattacharyya, *RSC Adv.*, 2014, **4**, 28537–28586
- 24 H.M.F. Freundlich, *Z. Phys. Chem.*, 1906, **57**, 385–470.
- 25 Y. S. Ho, *J. Hazard. Mater.*, 2006, **B136**, 681–689.
- 26 Y.S. Ho and G. McKay, *Process Biochemistry*, 1999, **34**, 451–465.
- 27 L. C. Lin and R. S. Juang, *Chem. Eng. J.*, 2007, **132**, 205–213.
- 28 Y. Prasanna Kumar, P. King, V.S.R.K. Prasad, *J. Hazard. Mater.*, 2006, **137**, 1211–1217.

Tables

Tab. 1 The adsorption properties of 732 IER, S-aTEPRs and S-bTEPRs.

Sample	IEC(meq·g ⁻¹)	WU or SD (%)
S-aTEPRs	1.63	18.05
S-bTEPRs	1.98	25.54
732 IER	2.21	27.69

Tab. 2 The elemental composition for each step of TG as for S-bTEPRs.

TG Steps	C Area	H Area	N Area	O Area	S Area
Intial	30296	14165	2803	21407	1662
First Step	30182	11402	2707	15730	1571
Second Step	9670	1529	1089	12574	793
Third Step	3062	427	112	2303	217

Tab. 3 XPS elemental compositions.

Samples	C 1s (285eV)	O 1s (533eV)	N 1s (400eV)	S 2p (168eV)
bTEPRs	84.23	10.62	5.51	—
S-bTEPRs	52.18	29.47	9.77	8.58

Tab. 4 Parameters of Langmuir and Freundlich isotherms for the ion exchange of metals on S-bTEPRs.

	Langmuir constants			Freundlich constants		
	$Q_0(\text{mg}\cdot\text{g}^{-1})$	$b(\text{L}\cdot\text{mg}^{-1})$	R^2	k_f	$1/n$	R^2
Ca(II)	23.30	0.13	0.9981	41.85	0.050	0.7855
Cu(II)	56.27	0.16	0.9983	23.45	0.066	0.8476

Tab. 5 Parameters for the pseudo-second-order kinetic model.

Metal	T (K)	$q_{e,exp}^*$ ($\text{mg}\cdot\text{g}^{-1}$)	$k_2\times 10^{-4}$ ($\text{g}\cdot\text{mg}^{-1}\cdot\text{min}^{-1}$)	q_e ($\text{mg}\cdot\text{g}^{-1}$)	R^2
Ca(n)	298	35.49	7.9021	33.31	0.9968
	318	36.06	9.4898	35.31	0.9974
	338	36.74	13.7276	36.46	0.9985
Cu(n)	298	43.76	6.6763	39.43	0.9946
	318	44.86	7.3414	40.21	0.9955
	338	45.73	7.9477	40.87	0.9953

* Amount of metal adsorbed for 24 h which can be considered as the equilibrium absorption capacity because there is no change with more time.

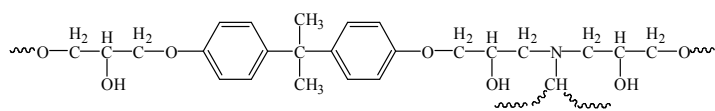


Fig. 1 Structure of thermosetting epoxy resin



Fig. 2 Photographs of aTEPRs, bTEPRs and the sulfonated products of S-aTEPRs and S-bTEPRs. (a) aTEPRs, (b) S-aTEPRs, (c) bTEPRs, (d) S-bTEPRs.

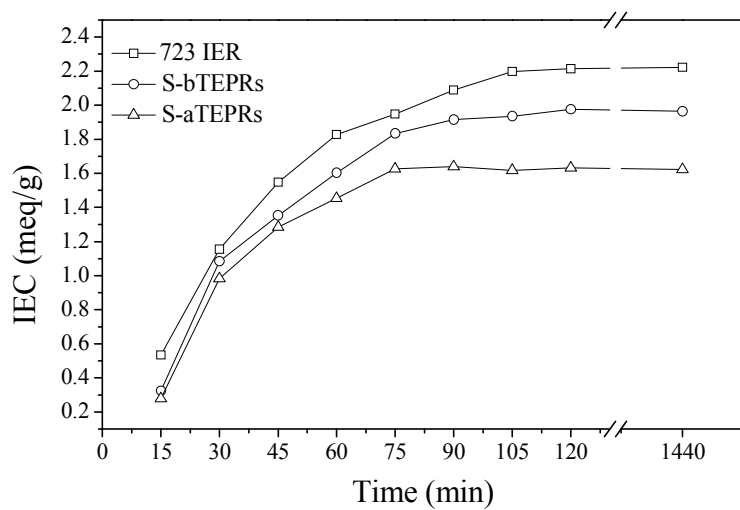


Fig. 3 IEC of 723 IER, S-aTEPRs and S-bTEPRs with time at ambient temperature.

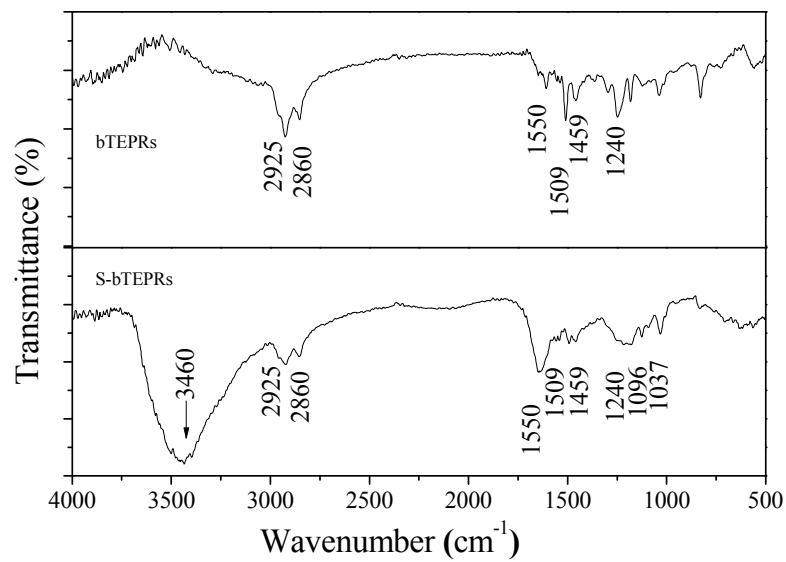


Fig. 4 FTIR spectra of bTEPRs and S-bTEPRs.

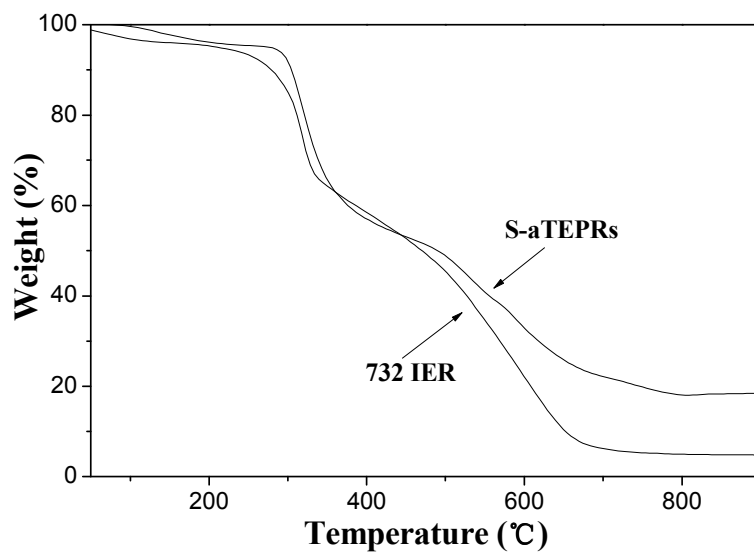


Fig. 5 TG curves of 732 IER and S-aTEPRs (10 °C/min, N₂: 50 mL/min).

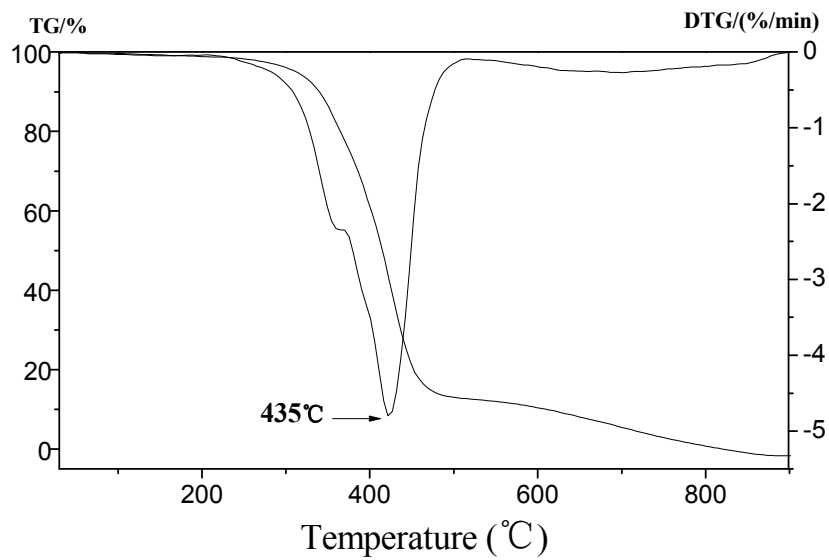


Fig. 6 TG-DTG curves of bTEPRs (10 °C /min, N₂: 50 mL/min).

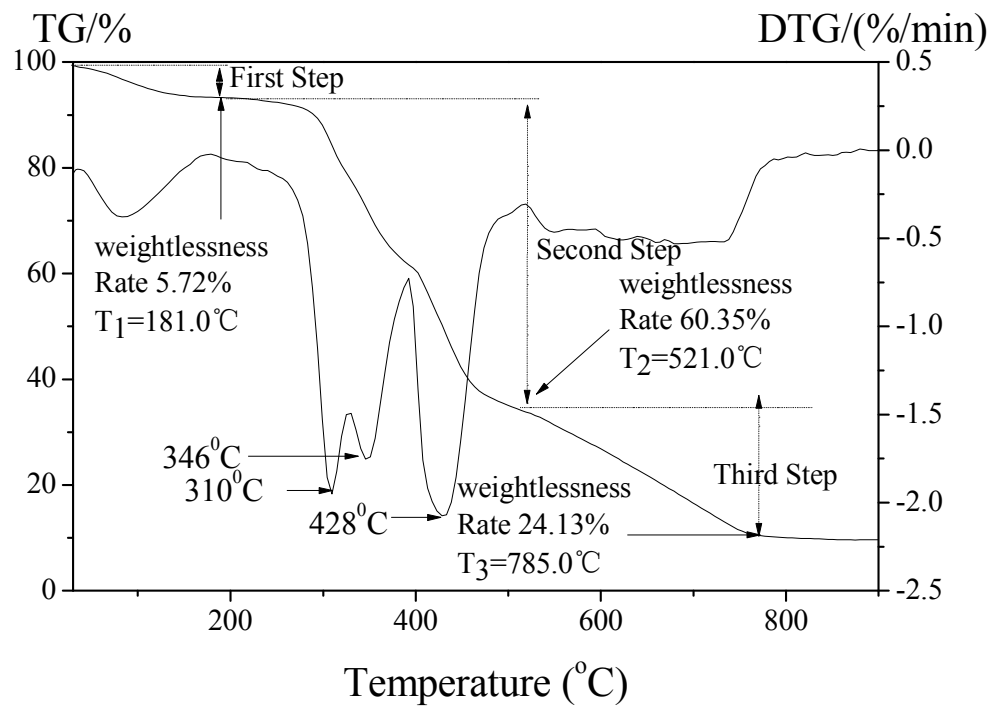


Fig. 7 TG-DTG curves of S-bEPRs (10 °C /min, N₂: 50 mL/min).

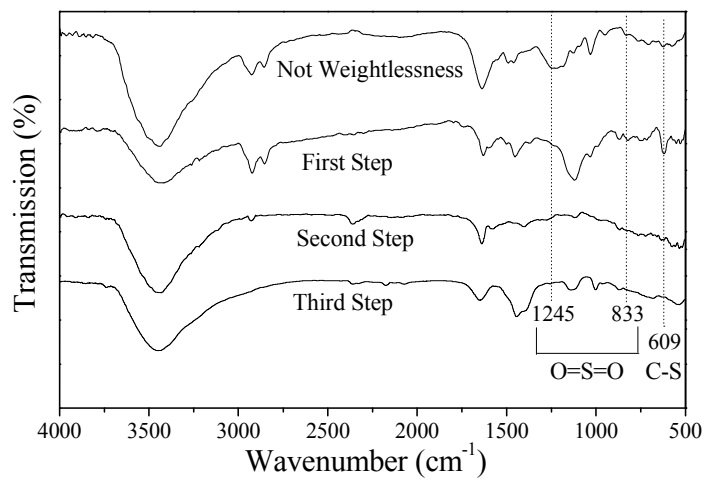


Fig. 8 FTIR spectra of different weight loss steps in S-bTEPRs.

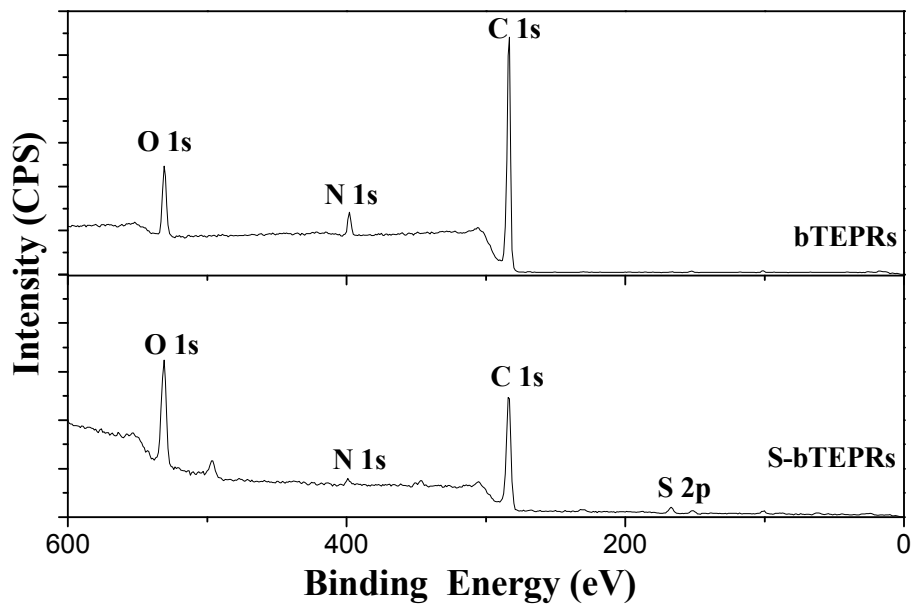


Fig. 9 The XPS wide scan spectra of bTEPRs and S-bTEPRs.

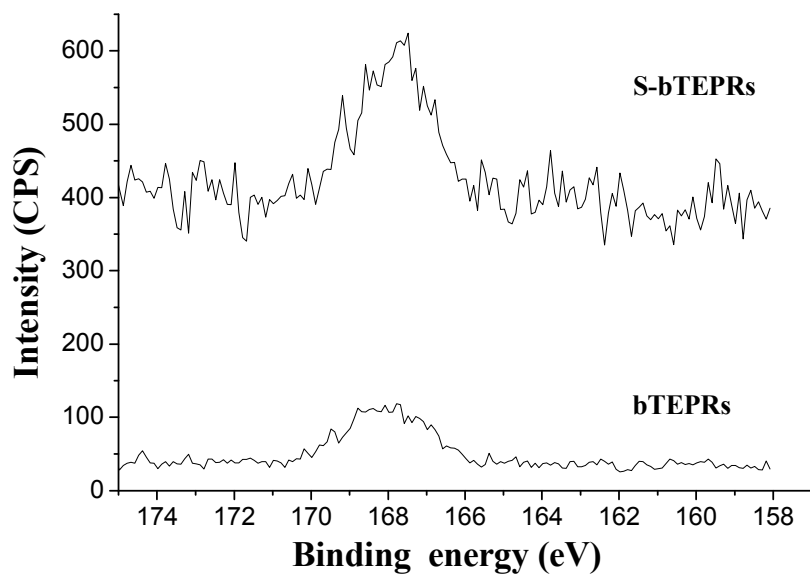


Fig. 10 The XPS narrow S 2p scan spectra of bTEPRs and S-bTEPRs.

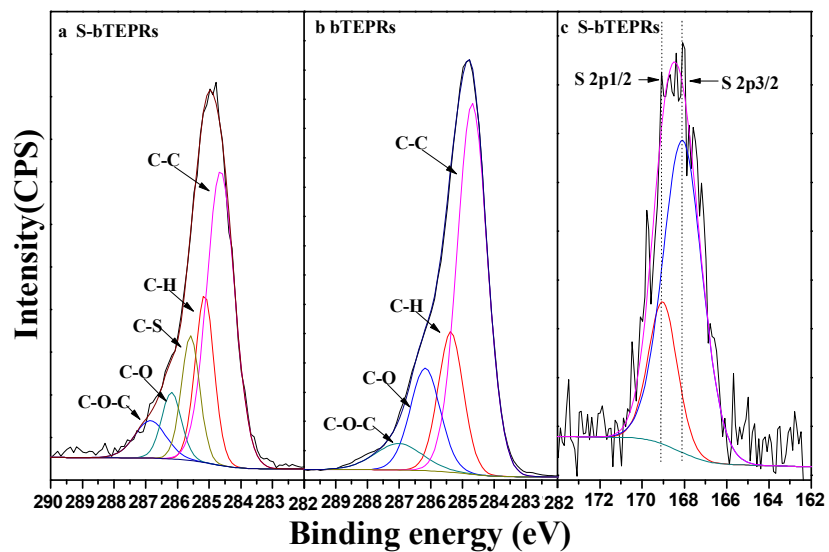


Fig. 11 The XPS narrow scan spectra and fit curves. (a) C 1s of the S-bTEPRs, (b) C 1s of the bTEPRs, (c) S 2p of the S-bTEPRs.

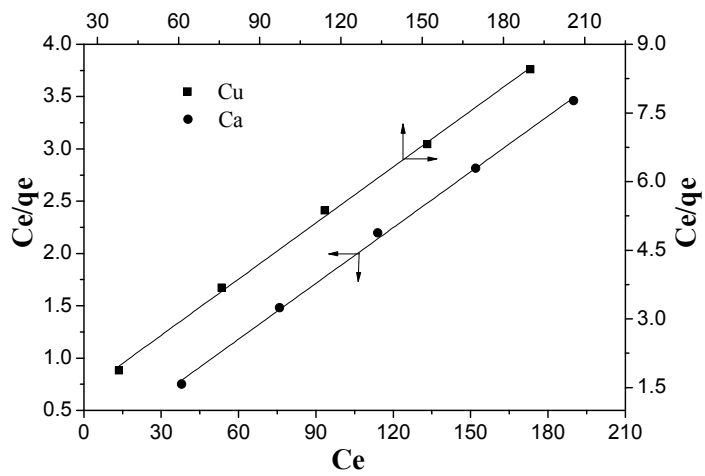


Fig. 12 Langmuir isotherm for ion exchange of Cu(II) and Ca(II) in S-bTEPRs.

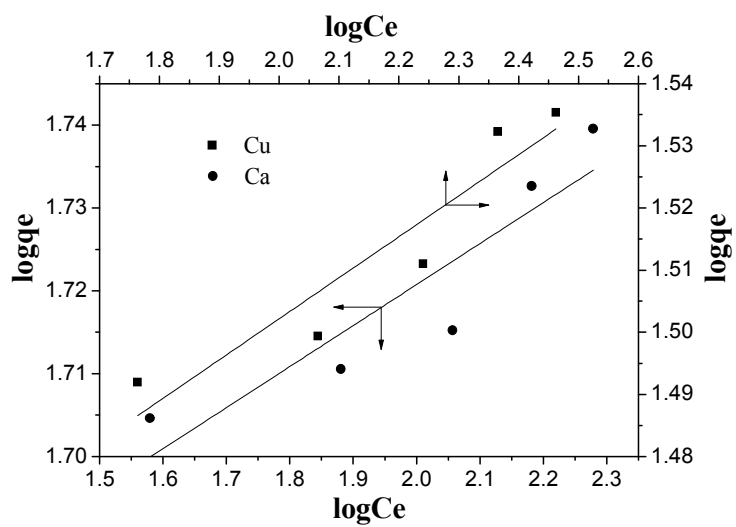


Fig. 13 Freundlich isotherm for ion exchange of Cu(II) and Ca(II) in S-bTEPRs.

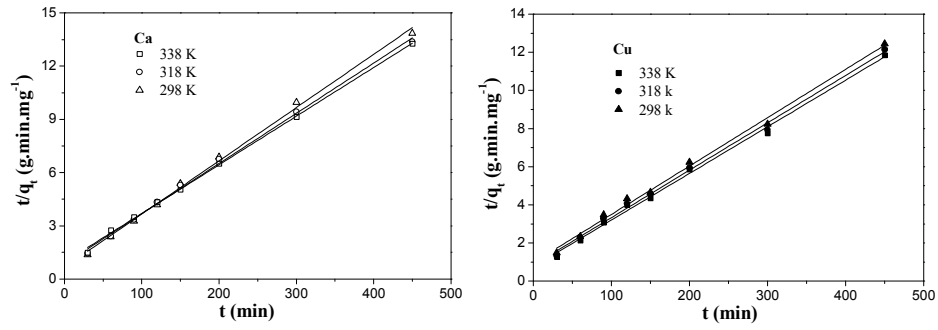


Fig. 14 The fit curves of the pseudo-second-order equation for adsorption of Ca(II) and Cu(II) in S-bTEPRs at different temperatures.

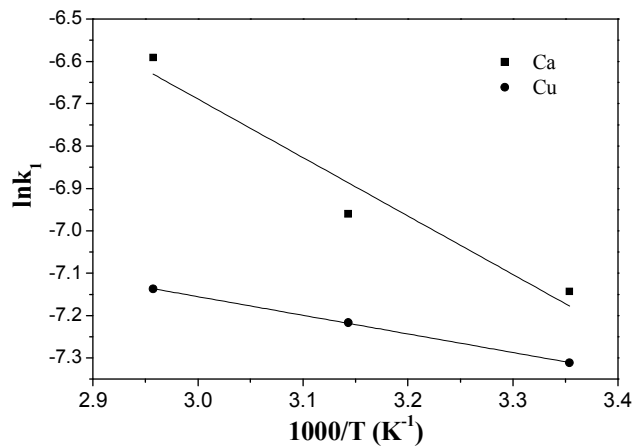


Fig. 15 Relationship between reaction rate constants and temperature for adsorption of Cu(II) and Ca(II) in S-bTEPRs